 CMES, vol.118, no.1, pp.91-109, 2019

A Trajectory Planning-Based Energy-Optimal Method for an EMVT System

Jiayu Lu[1] and Siqin Chang[1, *]

Abstract: In this paper, a trajectory planning-based energy-optimal method is proposed to reduce the energy consumption of novel electromagnetic valve train (EMVT). Firstly, an EMVT optimization model based on state equation was established. Then, the Gauss pseudospectral method (GPM) was used to plan energy-optimal trajectory. And a robust feedforward-feedback tracking controller based on inverse system method is proposed to track the energy-optimal trajectory. In order to verify the effectiveness of the energy-optimal trajectory, a test bench was established. Finally, co-simulations based on MATLAB Simulink and AVL Boost were carried out to illustrate the effect of energy-optimal trajectories on engine performance. Experimental results show that the robust tracking controller can achieve good position tracking performance. And these energy-optimal trajectories can save up to 40% of the energy consumption compared with the conventional camshaft valve trajectories.

Keywords: Electromagnetic valve train, energy optimization, trajectory plan, robust tracking control, co-simulation.

1 Introduction

Electromagnetic valve train (EMVT) can achieve fully flexible control of the valve, which means that the valve lift, the valve duration and the valve timing are regulated flexibly [Liu and Chang (2009)], and therefore the engine performance is improved significantly. However, since EMVT needs to consume additional electrical energy, the study on the energy optimization of EMVT is of great significance.

Most research published currently focus on reducing energy consumption of EMVT by optimizing the structure of EMVT [Olyaie, Razfa, Wang et al. (2011)]. A multi-objective optimal design was done by the Finite Element Analysis, on the basis of the dynamics model of EMVT in Yang et al. [Yang, Liu, Ye et al. (2013)]. Multiple objectives, such as magnetic holding force, release current and rising time are optimized, to achieve the energy consumption saving. In Hey et al. [Hey, Teo, Bui et al. (2014)], an output space mapping technique is used to replace the finite element analysis to solve the optimization problem. And an optimization geometric configuration of a flexure-based electromagnetic actuator is proposed to reduce the conversion losses. The structure of the EMVT studied in this paper has also been optimized. The electromagnetic field is optimized by optimizing the

[1] School of Mechanical Engineering, Nanjing University of Science and Technology, Nanjing, 210094, China.

* Corresponding Author: Siqin Chang. Email: siqinchang@126.com.

CMES. doi:10.31614/cmes.2019.04190 www.techscience.com/cmes

permanent magnet array and armature reaction. In this way, the output force is increased [Liu (2009); Tan, Li, Ge et al. (2018)]. However, with the development of the research, the room for further reducing the energy consumption by optimizing the actuator structure is very small.

Besides, trajectory planning is an effective energy optimization method for servomotor system [Huang, Hsu and Fung (2012)]. So we focus on the trajectory planning to further reduce the energy consumption of EMVT. In Wang et al. [Wang, Ueda and Bortoff (2013)], the energy-optimal trajectory generation of servomotor system was discussed. And a decomposition-based shooting method was proposed to solve a nonlinear constrained optimal problem for servomotor systems. However, this method could not solve the optimal problem with acceleration constraint. A real-time energy-optimal trajectory generation method for a servomotor system when the system was subject to acceleration and speed constraints was proposed by Wang et al. [Wang, Zhao, Bortoff et al. (2015)]. The work done by Chen [Chen (2016)] used the sliding mode control and minimum-energy control to solve the optimal problem for a mechatronic motor-table system. An online minimum-energy translational and rotational velocity trajectory planning and control system was presented by Kim et al. [Kim and Kim (2014)] for three-wheeled omnidirectional mobile robots. However, none of these methods mentioned above are suitable for EMVT, because EMVT is suffering from exhaust pressure.

A trajectory planning-based energy-optimal method is proposed to reduce the energy consumption of a novel EMVT. Firstly, the mathematical model of EMVT and the cost function of energy consumption are established. Then, the Gauss pseudospectral method (GPM) is used to plan energy optimal motion trajectory. After the energy-optimal trajectories are generated, a robust feedforward-feedback controller based on inverse system method is proposed to track the energy-optimal trajectories. Additionally, to verify the effectiveness of the energy-optimal trajectories and the performance of the robust tracking control, a test bench is built. Finally, co-simulations based on MATLAB Simulink and AVL Boost are carried out to illustrate the effect of energy-optimal trajectory on engine performance. Experiment and co-simulation results show that these energy-optimal trajectories can effectively reduce the energy consumption of EMVT without affecting the engine performance.

2 Problem statement

2.1 Structure and mathematical model of EMVA

A prototype of the novel EMVT studied in this paper is shown in Fig. 1. The traditional camshaft is replaced by the EMVT on the engine, position sensors are used to measure the valve position. EMVT can realize all kinds of valve motion strategies, such as variable valve lift, variable valve timing and cylinder deactivation. The structure of EMVT is shown in Fig. 2. The EMVT consists of a moving coil, permanent magnets, a valve, an inner core and an outer core. The moving coil of EMVT is connected to the valve. The inner and outer cores form a uniform air gap magnetic field. The movement of the valve can be controlled by controlling the magnitude and direction of the coil current [Liu and Chang (2011)].

Figure 1: Prototype of EMVT

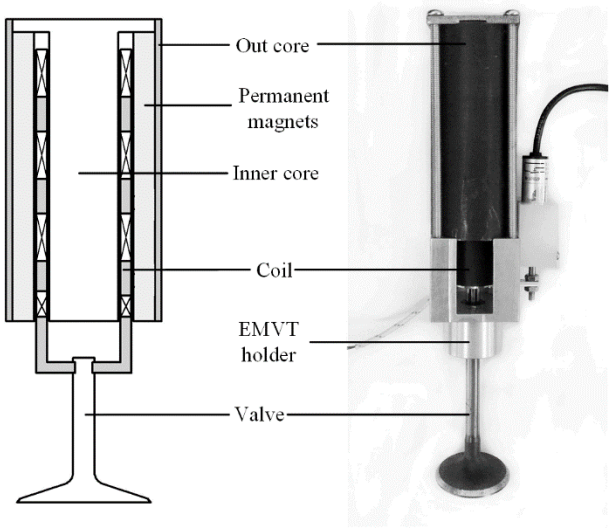

Figure 2: Schematic structure of the EMVT

The EMVA consists of electrical, magnetic and mechanical subsystems. The electrical subsystem is described as follow:

$$L\dot{i} = -Ri - K_e v + u \tag{1}$$

where u is the input phase voltage, i is the current through the coil, R , L represents the resistance and inductance of the coil respectively, K_e is the back electromotive force coefficient.

The magnetic and mechanical subsystems are described as follows:

$$\begin{cases} m\ddot{x} = F_m - F_d \\ F_m = K_m i \end{cases} \tag{2}$$

where m is the moving mass, x , $\dot{x}$ and $\ddot{x}$ denotes the position, the velocity and the acceleration of the mover respectively. F_m is the electromagnet force. K_m is the force sensitivity of the actuator, which denotes the ratio of the electromagnetic force to the input current. F_d represents the external disturbance, which is the uncertain nonlinearity of the system. Furthermore, in this EMVT system, K_m and K_e are approximately equal.

The disturbance force F_d in the intake valve mainly means frictional force, which is ignored compare with the electromagnetic force. However, due to the exhaust pressure in the exhaust valve, the disturbance force F_d can't be ignored. The disturbance force is described as :

$$\begin{cases} F_d = C_{gf} P_0 A_v f(x) \\ f(x) = e^{-600x} \end{cases} \tag{3}$$

where C_{gf} is the gas force coefficient that simulates the effect of flow losses behind the valve during opening. A_v is the valve face area. P_0 is the initial pressure of the exhaust valve. C_{gf} was found to range from approximately 0.85-0.7 over the valve stroke [Chladny and Koch (2008)].

The EMVT parameters used in this paper are shown in Tab. 1.

Table 1: Parameters of the EMVT

Parameter	Valve
R	1.38 Ω
L	0.94 mH
K_e	12 $V \cdot s/m$
K_m	12 N/A
m	94.6 g
A_v	4.45*10^{-4} m^2
C_{gf}	0.8-0.75

2.2 Valve motion of the EMVT

The valve motion trajectory of the EMVT is shown in Fig. 3, which consists of three phases: opening-phase 1, keeping-phase 2 and closing-phase 3. In the intake valve, the external disturbances can be ignored compared with the electromagnetic force. However, the exhaust valve will suffer from an additional exhaust pressure during the opening-phase 1. And the exhaust pressure can be ignored in keeping-phase 2 and closing-phase 3. The robust controller works only in opening-phase 1 and closing-phase 3. A fixed current is applied during the keeping-phase 2 to ensure the stability of the valve [Fan, Liu, Chang et al. (2016)].

The travel process of the intake valve is similar to that of the exhaust valve when the initial exhaust pressure is 0 bar. Therefore, only the exhaust valve travel process is studied in this paper.

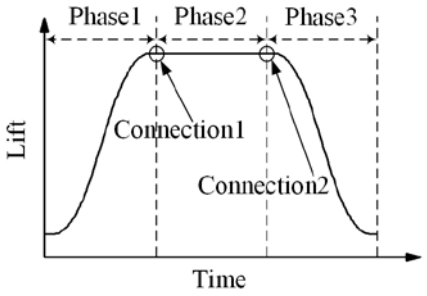

Figure 3: Valve motion of the EMVT

2.3 Optimization modeling of the EMVT

In order to achieve optimal energy consumption of the EMVT, an appropriate cost function is needed. The function we has optimized in this paper is the minimum input electrical energy, described as follow:

$$E = \int_{t_0}^{t_f} uidt \tag{4}$$

where t_0 is the initial time, t_f is the final time.

The input electrical energy contains three parts: copper loss, iron loss and mechanical loss.

$$W_{elec} = W_{cu} + W_{fe} + W_{mech} \tag{5}$$

where W_{elec}, W_{cu}, W_{fe} and W_{mech} represents the input electrical energy, copper loss, iron loss and mechanical loss respectively.

The study done by Dai et al. [Dai and Chang (2014)] indicated that the ratio of copper loss to iron loss of the EMVT is obtained as 7:3. Therefore, in order to simplify the calculation of optimal trajectory planning for energy consumption, a new cost function Eq. (6) is selected for the optimization problem. In Eq. (6), only copper loss and mechanical loss are included.

$$E_0 = \int_{t_0}^{t_f} (i^2 R + K_m iv)dt \tag{6}$$

Then the valve position x, the valve velocity v and coil current i are set as the state variables in this paper, $x = [x_1, x_2, x_3]^T = [x, v, i]^T$. The input voltage u is set as the control variable. Combining with Eq. (1) and Eq. (2), the mathematical model of EMVA are translated into first-order differential-algebraic equations, which are described as follows:

$$\begin{cases} \dot{x}_1 = x_2 \\ \dot{x}_2 = (K_m/m)\cdot x_3 - (K/m)\cdot x_1 - F_f/m \\ \dot{x}_3 = -(R/L)\cdot x_3 - (K_e/L)\cdot x_2 + u/L \end{cases} \tag{7}$$

Table 2: Constraints of the parameters

constraints	Parameters	Values
Boundary conditions	Initial position	0
	Final position	8 mm
	Initial time	0
	Final time	t_f
Path constraints	Valve velocity	≤10 m/s
	Valve acceleration	≤4000 m/s^2
	Input voltage	≤42 V

In order to make the optimization model available, the valve velocity, valve acceleration and input voltage must be limited at suitable range. The path and boundary constraints of the EMVT are shown in Tab. 2.

3 Optimization method

The theory of optimal control has been developed for a long time, but the algorithms for solving nonlinear optimal control problems accurately and efficiently are still limited. Generally, to solve the trajectory optimization problem, the current methods can be divided into two categories: indirect methods and direct methods Betts (1998)]. The pseudospectral (PS) method approximates the control and state variables through global interpolation polynomials, then discrete the optimal control problem (OCP) to a nonlinear programming problem (NLP) effectively. It is a kind of direct method with more solving efficiency [Elnagar, Kazemi and Razzaghi (1995); Yang, Cui, Hao et al. (2017)]. In the last decade, PS methods, such as Legendre PS method, Gauss PS method and Radau PS method, have emerged as effective and flexible approaches to solve nonlinear optimal control problems [Garg, Patterson, Hager et al. (2017)]. The Gauss pseudospectral method (GPM) is used in this paper, which shows promise in the numerical solution of OCP.

Consider the following fairly general OCP as the continuous Bolza form.

$$\begin{aligned} &\dot{x}(t) = f(x(t),u(t),t) \\ &\min J = \phi(x(t_f),t_f) + \int_{t_0}^{t_f} G(x(t),u(t),t)dt \end{aligned} \tag{8}$$

where J is the cost function, $\phi \in R$ is Mayer cost function, $G \in R$ is Lagrange cost function.

The basic steps for GPM to solve the OCP are shown as follows:

Step 1: Change the time interval of the OCP from $t \in [t_0, t_f]$ to $\tau \in [-1,1]$, to satisfy the defined interval of the interpolation polynomials.

$$\tau = \frac{2t - t_f - t_0}{t_f - t_0} \tag{9}$$

Step 2: GPM discretization of the OCP. The GPM is assigned to Legendre-Gauss (LG)

point, the LG point does not include the intial point and the end point.

$$\tau_0,\ldots,\tau_{N-1},\tau_i\in[-1,1],(i=0,\cdots,N-1) \tag{10}$$

Then, the state and control variables are discreted at the LG point, the Lagrange polynomial is used to approximate the state and control variables.

$$\begin{aligned} x(\tau)&\approx X(\tau)=\sum_{i=0}^{N}L_i(\tau)X_i \\ u(\tau)&\approx U(\tau)=\sum_{i=0}^{N}L_i(\tau)U_i \end{aligned} \tag{11}$$

where $L_i(\tau)$ are Lagrange polynomial basis function, which can be described as:

$$L_i(\tau)=\prod_{j=0,j\neq i}^{N}\frac{\tau-\tau_j}{\tau_i-\tau_j} \tag{12}$$

Step 3: State function transformation. After the state variables are discreted by the Lagrange polynomial, the differential operation of the state can be approximated as a differential operation on the interpolation basis function.

$$\sum_{i=0}^{N}D_{ki}X_i-\frac{t_f-t_0}{2}f(X_k,U_k,\tau_k)=0 \tag{13}$$

where $k=0,1,\cdots,N$; D_{ki} are differential matrices, which represent the differential values of each Lagrange basis function at each LG point.

$$D_{ki}=\dot{L}_i(\tau_k)=\sum_{\substack{i=0\\l\neq i}}^{N}\frac{\prod_{j=0,j\neq i,l}^{N}\tau_k-\tau_j}{\prod_{j=0,j\neq i}^{N}\tau_i-\tau_j} \tag{14}$$

Step 4: Cost function transformation. The continuous cost function is approximated using a Gauss quadrature as

$$J=\phi\left[X(\tau_0),t_0,X(\tau_f),t_f\right]+\frac{t_f-t_0}{2}\sum_{i=0}^{N}w_iG(X_i,U_i,\tau_i) \tag{15}$$

where w_i are the Gauss weight.

Finally, the original continuous optimal control problem is transformed into the nonlinear programming problem. The control variable and state variables at the LG points are needed to be opimized.

$$\begin{aligned} &\min J=\phi\left[X(\tau_0),t_0,X(\tau_f),t_f\right]+\frac{t_f-t_0}{2}\sum_{i=0}^{N}w_iG(X_i,U_i,\tau_i) \\ &\left\|\sum_{i=0}^{N}D_{ki}X_i-\frac{t_f-t_0}{2}f(X_k,U_k,\tau_k)\right\|_\infty\leq\delta \end{aligned} \tag{16}$$

Interested readers are referred to Benson [Benson (2005)] for specific process.

4 Tracking controller and experimental setup

A robust feedforward-feedback tracking controller based on inverse system method is proposed to track the energy-optimal trajectory and an experimental setup is built to

verify the effectiveness of the energy-optimal trajectories.

4.1 Tacking controller

The struture diagram of the tracking controller is shown in Fig. 4. Fistly, according to the target valve movement time t_d, the initial exhaust valve pressure P_0 and the target valve lift x_d, the optimal valve lift curves x^* are obtained by utilizing the GPM mentioned above. The traget lift x_d means the final position x_f in the OCP, which is 8 mm in this paper. The valve movement time means the final time t_f in the OCP, which is changed with the engine speed. The the optimal valve lift curve x^* is feed through a low-pass filter to eliminate high frequency compoents and produce the reference position, speed, acceleration and jerk trajectories denoted by x_r, v_r, a_r, a'_r. According to the reference x_r, v_r, a_r, a'_r and measured position signal, the control voltage u is obtained by the tacking controller, and finally acts on the EMVT.

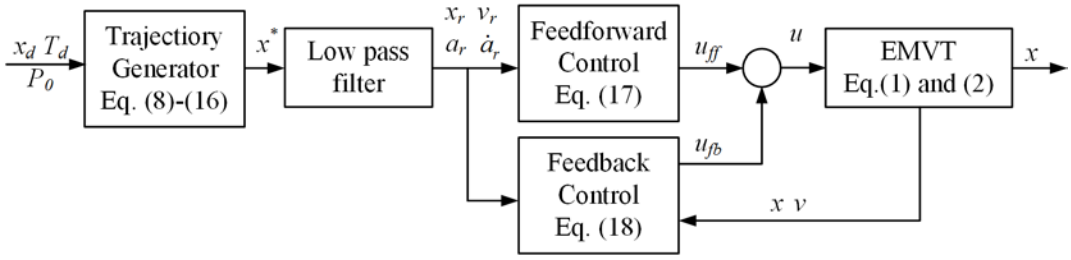

Figure 4: The structure diagram of the tracking controller

The tracking controller consists of a feedforward u_{ff} and a feedback u_{fb}. The feedforward u_{ff} is obtained by the inverse system method, which is based on the Eqs. (1), (2). It can be expressed as the following form [Cui, Ju, Zhou et al. (2014)]:

$$u_{ff} = \frac{mL}{K_m}\dot{a}_r + \frac{Rm}{K_m}a_r + K_e v_r + \frac{RC_{gf}P_0A_v}{K_m}e^{-600x} \tag{17}$$

The feedback u_{fb} is a proportional-derivative (PD) control. It can be expressed as the following form [Zhao (2018)]:

$$u_{fb} = k_x(x_r - x) + k_v(v_r - v) \tag{18}$$

where k_x, k_v are constant control parameters. The control voltage u is obtained as follow:

$$u = u_{ff} + u_{fb} \tag{19}$$

4.2 Experimental setup

Due to the limitation of the test conditions, the EMVT can not be used in the actual working engine yet. Therefore, an experimental setup based on the EMVT prototype is built to verify the effectiveness of the energy-optimal trajectory. And an electromagnetic load simulator (EMLS) is connected to the EMVT which is used to simulate the

combustion force by controlling the magnitude and direction of the coil current. In order to ensure the reliability of the experiment results, the moving mass of the EMLS is consistent with the valve mass. Experimental setup of the EMVT system is shown in Fig. 5.

A digital signal processor (TMS320F2812) is used as the digital controller which has a clock frequency of 150 MHz. A position sensor (LCIT series) with a range of 10 mm and a bandwidth of 1 kHz is used to provide the position feedback. Two current sensors (ACS712) and voltage snesors are used to take the currents measurement and voltages measurement respectivly which are integrated together with the PWM inverters. A force sensor (LSR series) is used to measure the simulated combustion force. Two 50 KHz PWM signals are used to switch the IGBT H-bridge and provide voltages between -42 V and +42 V to actuator. A Personal Computer is used to deal with the data received from the DSP by the Ethernet communication.

A well tuned proportional-integral-derivative (PID) controller is used for the EMLS. And the experimental results of the EMLS when the initial pressures are 1 bar, 3 bar and 5 bar respectively are shown in Fig. 6. As shown in Fig. 6, by controlling the current of the EMLS, the combustion force can be well tracked. And the maximum pressure error are within 10 N. So the EMLS can be used to simulate the combustion force in the experiments.

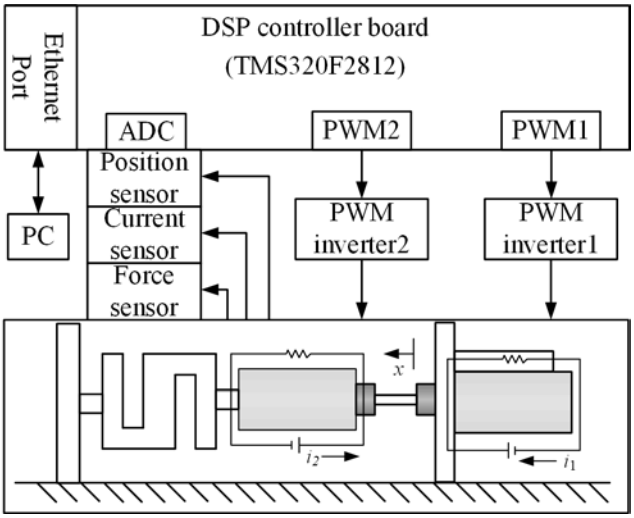

(a)

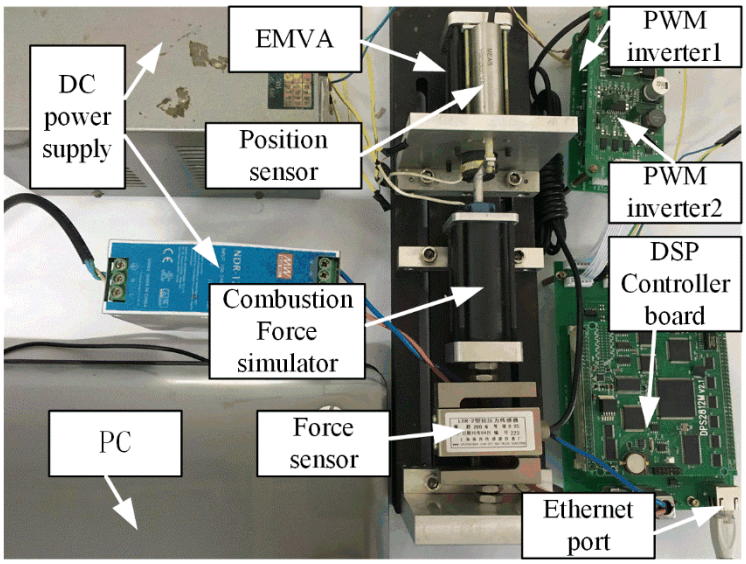

(b)

Figure 5: Experimental setup of the EMVA control system. (a) Schematic. (b) Actual. DC: direct current; ADC: analog-to-digital converter

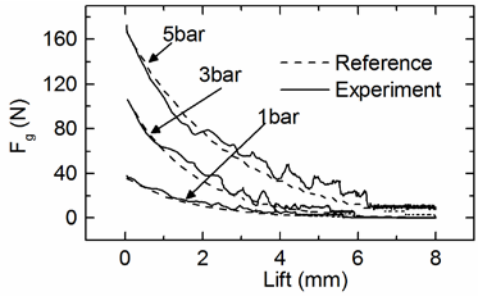

Figure 6: Control results of the electromagnetic load simulator

4.3 Tracking control results

In order to verify the performance of the tacking controller, experiments are carried out when the initial exhaust pressure is 3 bar and the valve travel time is 8 mm. A traditional camshaft valve trajectory is used to compare with the energy-optimal trajectory. The experiment tracking results are shown in Fig. 7, the tracking errors are shown in Fig. 8. According to Fig. 7, although there is a little difference in the tacking performance between the energy-optimal trajectory and the conventional camshaft valve trajectory, the difference is not remarkable. In Fig. 8, the tracking errors of both trajectories are within 0.15 mm, which show that the tracking controller has a good tracking performance for both trajectories.

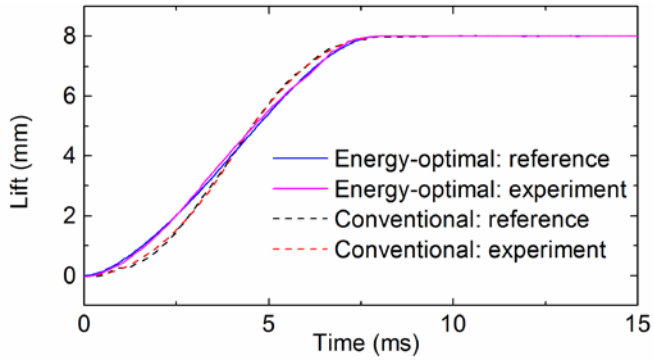

Figure 7: Experiment results of two different trajectories

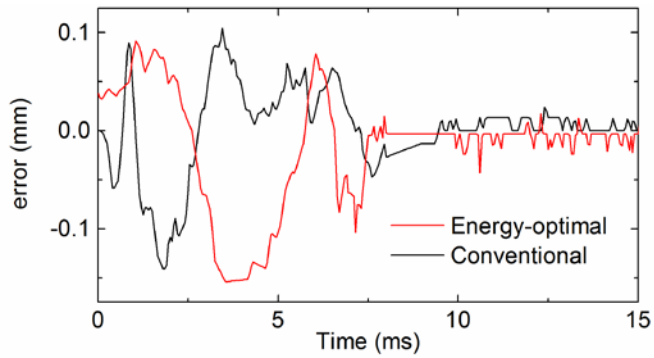

Figure 8: Tracking errors of two different trajectories

5 Experiment results and discussion

In conventional camshaft engines, the valve travel time is related to engine speed. However, in the EMVT engine, the valve travel time can be regulated flexibly. Therefore, the engine speed is replaced by the valve travel time in this paper, to illustrate the different operating conditions of the engine. 36 cases are listed in this paper to fully illustrate the effectiveness of the energy-optimal trajectories under different engine operating conditions.

5.1 Trajectory planning results

The trajectories planning are carried out for the cases where the valve travel time is 5, 6, 7, 8, 9, 10 ms and the initial exhaust pressure is 0, 1, 2, 3, 4, 5 bar respectively. The energy-optimal opening trajectories and the conventional camshaft valve trajectories when the initial exhaust pressure is 3 bar are shown in Fig. 9. The exhaust pressure is negligible during the closing process of the exhaust valve. The closing trajectories are shown in Fig. 10.

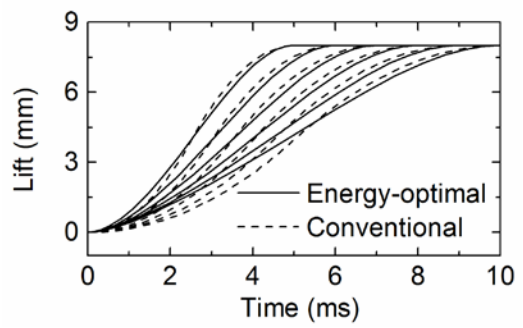

Figure 9: Opening trajectories when the initial exhaust pressure is 3 bar

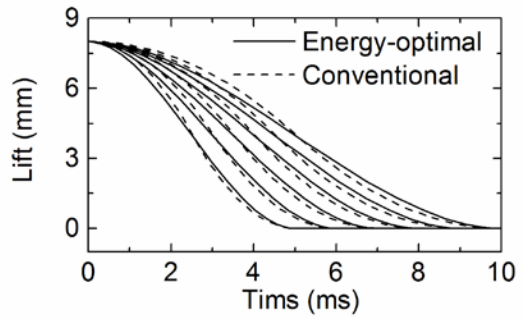

Figure 10: Closing trajectories of the exhaust

5.2 Experiment results

After the trajectories are planned, the trajectory tracking controller is used to track the trajectories. Finally, the tests are done on the experimental setup. The position signals, current signals and voltage signals of the EMVT are transmitted to the PC through Ethernet communication. The energy consumption of the EMVT can be obtained by analysing these dates.

According to Eq. (5), the total input electrical energy W_{elec} of the EMVT system consists of two parts,

$$W_{elec} = W_e + W_{mech} \tag{20}$$

where W_e represent the total internal losses of the EMVT, which includes the copper losses W_{cu} and the iron losses W_{fe}. W_{mech} represents the work done by the EMVT to overcome the exhaust pressure.

Tab. 3 lists the energies consumed by the opening process of the exhaust valve with the energy-optimal trajectories. Tab. 4 lists the energies consumed by the opening process of the exhaust valve with the conventional valve trajectories. The energies consumed by the closing process of exhaust valve are almost the same as the energy consumed by the exhaust valve opening process when the initial exhaust pressure is 0 bar, and they are shown in Tab. 5.

Table 3: Energies consumption of EMVT with the optimal trajectories

case	5 ms		6 ms		7 ms		8 ms		9 ms		10 ms	
	We	*Wg*	*We*	*Wg*	*We*	*Wg*	*We*	*Wg*	*We*	*Wg*	*We*	*Wg*
0 bar	0.50	0.52	0.29	0.37	0.19	0.27	0.13	0.21	0.09	0.17	0.07	0.15
1 bar	0.61	0.57	0.39	0.42	0.28	0.32	0.22	0.26	0.18	0.22	0.16	0.20
2 bar	0.74	0.62	0.52	0.46	0.40	0.37	0.34	0.31	0.31	0.27	0.29	0.25
3 bar	0.90	0.66	0.67	0.51	0.56	0.42	0.50	0.36	0.47	0.32	0.45	0.30
4 bar	1.08	0.71	0.85	0.56	0.74	0.47	0.68	0.41	0.66	0.37	0.64	0.35
5 bar	1.27	0.75	1.04	0.60	0.94	0.51	0.89	0.46	0.87	0.42	0.86	0.40

Table 4: Energies consumption of EMVT with the conventional valve trajectories

case	5 ms		6 ms		7 ms		8 ms		9 ms		10 ms	
	We	*Wg*	*We*	*Wg*	*We*	*Wg*	*We*	*Wg*	*We*	*Wg*	*We*	*Wg*
0 bar	0.77	0.92	0.45	0.64	0.29	0.48	0.20	0.37	0.15	0.30	0.11	0.24
1 bar	0.92	0.97	0.58	0.69	0.41	0.53	0.32	0.42	0.26	0.35	0.22	0.30
2 bar	1.10	1.02	0.75	0.74	0.58	0.58	0.48	0.48	0.42	0.40	0.39	0.35
3 bar	1.31	1.07	0.96	0.80	0.79	0.64	0.70	0.53	0.65	0.46	0.62	0.40
4 bar	1.55	1.13	1.21	0.85	1.04	0.69	0.96	0.59	0.93	0.51	0.92	0.46
5 bar	1.83	1.18	1.49	0.91	1.34	0.75	1.28	0.64	1.27	0.57	1.28	0.52

Table 5: Energies consumption of the clsosing process

case	5 ms		6 ms		7 ms		8 ms		9 ms		10 ms	
	We	*Wg*	*We*	*Wg*	*We*	*Wg*	*We*	*Wg*	*`We*	*Wg*	*We*	*Wg*
opt	0.49	0.54	0.27	0.40	0.20	0.25	0.15	0.24	0.11	0.16	0.08	0.17
con	0.76	0.95	0.46	0.67	0.27	0.50	0.22	0.39	0.17	0.29	0.14	0.26

In order to explain the variations of energy consumptions under different cases, the total energies consumption of the EMVT system are shown in Fig. 11 and Fig. 12. The following information can be obtained from Tabs. 3, 4 and Figs. 11, 12.

(1) The energy consumption varies from case to case. However, the energy consumption changing rules with the initial exhaust pressure and the valve travel time of the energy-optimal trajectory EMVT system are basically consistent with the conventional trajectory EMVT system.

(2) Under the same initial exhaust pressure, the shorter the valve travel time, the greater the energy consumption. Because a larger current is required to achieve lager valve travel acceleration, which lead to a greater internal loss of the EMVT system. Meanwhile, when the valve travel time becomes shorter, the motion speed of the EMVT should be faster, which leads to an increase of the mechanical loss.

(3) Under the same valve travel time, the smaller the initial exhaust pressure, the less the

energy consumption. This is because the lager the initial exhaust pressure, the more current is needed to overcome the exhaust pressure, which leads to an increase of the internal loss of the EMVT. And due to the increase in exhaust pressure, the mechanical losses of the EMVT system will also increase.

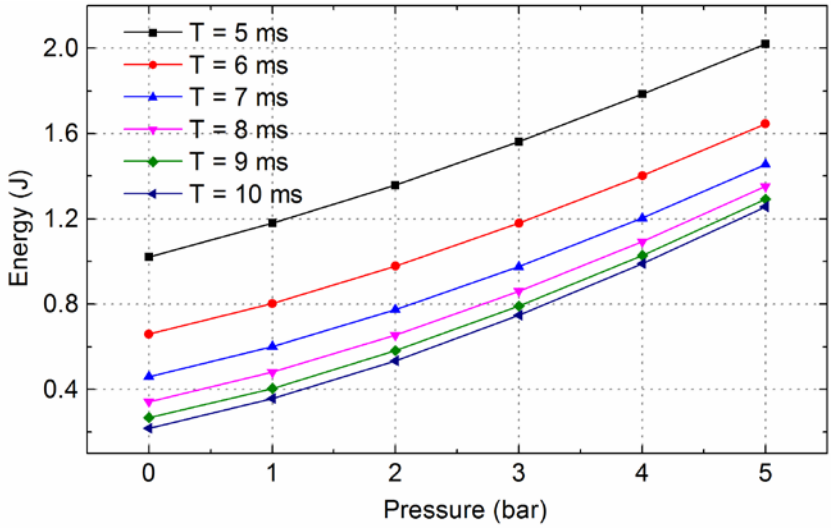

Figure 11: Energies consumption of EMVT with the energy-optimal trajectories

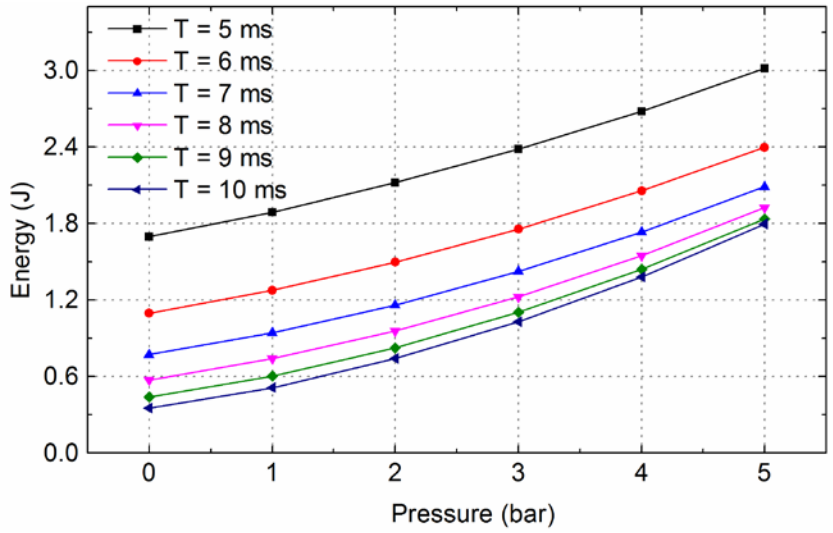

Figure 12: Energies consumption of EMVT with the conventional trajectories

The energy-saving efficiencies of the EMVT system are shown in Fig. 13. As shown in Fig. 13, the energy-saving efficiencies varies from case to case. For all 36 cases, the energy-saving efficiencies are between 27% and 40%. Under the same initial exhaust pressure, the shorter the valve travel time, the greater the energy saving efficiency. And at the same valve travel time, the smaller the initial exhaust pressure, the greater the energy saving efficiency.

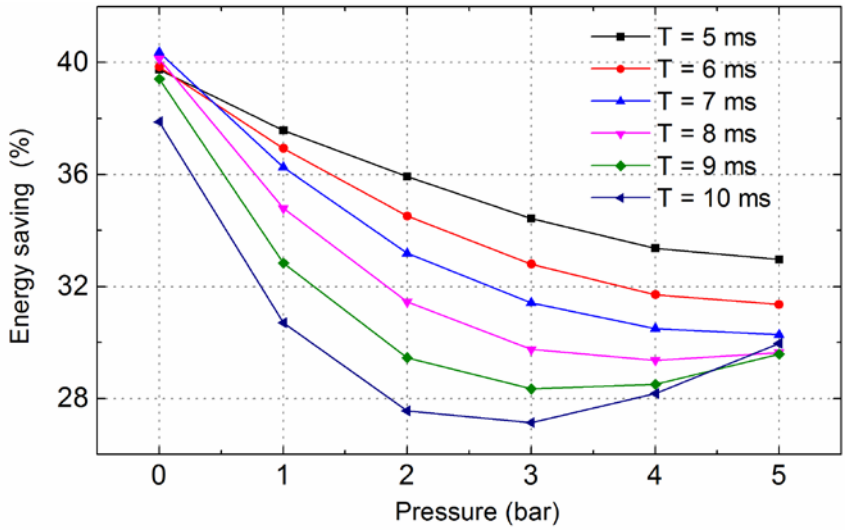

Figure 13: energy-saaving efficiencies of the EMVT system

6 Co-simulation and results analysis

The above contents verify the feasibility of the energy-optimal trajectories in energy saving. However, it is still necessary to verify whether the energy-optimal trajectories will affect the performance of the engine. In this paper, an integration simulation of MATLAB Simulink and AVL Boost is used to verify the impact of the energy-optimal trajectories on the engine performance.

6.1 Co-simulation framework

The EMVT dynamic and tracking control simulation are done in MATLAB Simulink to simulate the work process of the EMVT system. The EMVT system is modelled with Eq. (1) and Eq. (2). The tracking controller is modelled with Eq. (17) and Eq. (18). The detailed instructions of the EMVT dynamic and tracking controller simulation model are shown in Fig. 4. The engine studied in this paper is based on a 1.8L 4-cylinder inline gasoline engine. A one dimensional model of the prototype engine was carried out by using AVL Boost [Fan, Chang, Liu et al. (2016)]. And it has been proven that the actual operation of the prototype engine can be accurately simulated. The exhaust pressure and the engine speed of the EMVT system in the MATLAB Simulink simulation are obtained from AVL Boost. The EMVT motion curve obtained from the MATLAB Simulink simulation is uesd as the valve lift in AVL Boost. The structure of the co-simulation framework is shown in Fig. 14.

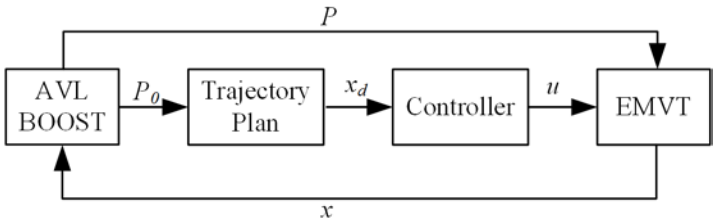

Figure 14: The structure of the co-simulation framework

6.2 Co-simulation results

Co-simulations of the prototype engine under different load conditions are carried out when the engine speed is 1000 rpm. The mean engine torque and brake specific fuel consumption (BSFC) are selected as evaluation indexs of the engine performance. Co-simulation results are shown in Fig. 15. Under the low load conditions, the mean engine torque of the engine with energy-optimal valve lift improve by 0.3% compared to that of the conventional camshaft valve lift. Under the high load conditions, the mean engine torque of the engine with energy-optimal valve lift decrease by 0.4%. The BSFC decrease by 0.2% under various loads. The performance of the engine with energy-optimal valve lift is indistinguishable from that of the engine with conventional camshaft valve lift.

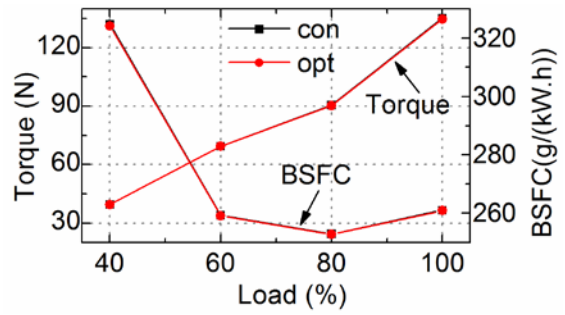

(a)

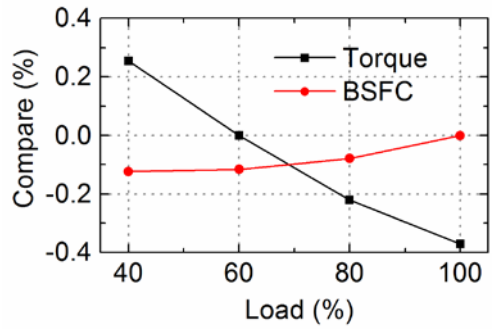

(b)

Figure 15: Co-simulation results

7 Conclusion

In this paper, an energy optimal method based on trajectory planning is proposed. A trajectory tracking controller combining with feedforward inverse system method and feedback PD controller is proposed to track the energy-optimal trajectories. An experimental setup is built to verify the effectiveness of the energy-optimal trajectories. In the experimental setup, an electromagnetic load simulator is used to simulate the combustion force. Finally, co-simulations based on MATLAB Simulink and AVL Boost are carried out to illustrate the effect of energy-optimal trajectory on engine performance. The main conclusions are as followings:

(1) An EMVT optimization model based on state equation is established. And the optimal control problem is solved by the Gauss pseudospectral method.

(2) An electromagnetic load simulator is used to simulate the combustion force. A well tuned proportional-integral-derivative controller is used to track the exhaust pressure. The experiment results show that EMLS can simulate the exhaust pressure well.

(3) A trajectory tracking controller combining with feedforward inverse system method and feedback PD controller is proposed. Satisfactory trajectory tracking performance is obtained by trial and error. The tracking errors are within 0.15 mm for both EMVT system with energy-optimal and conventional trajectories.

(4) The experiment results show that the energy-optimal trajectories can significantly reduce the energy consumption of the EMVT system. For all 36 cases, the energy-saving efficiencies are between 27% and 40%.

(5) The co-simulation results of MTALAB Simulink and AVL Boost show that the energy-optimal tajectories have little effect on the engine performance. The effect on the mean engine torque is witnin 0.4% and the effect on the BSFC is within 0.2%.

Acknowledgement: This work was supported by the National Natural Science Foundation of China (Grant Number 51306090).

References

Betts, J. T. (1998): Survey of numerical methods for trajectory optimization. *Journal of Guidance Control & Dynamics*, vol. 21, no. 2, pp. 193-207.

Benson, David. (2005): *A Gauss Pseudospectral Transcription for Optimal Control (Ph.D. Thesis)*. Massachusetts Institute of Technology, USA.

Cui, Y.; Ju, Y.; Zhou, C.; Liu, L.; Xu, J. (2014): Position control of linear electromechanical actuator for spoiler system base on the inverse system method. *Proceedings of the Institution of Mechanical Engineers Part G Journal of Aerospace Engineering*, vol. 228, no. 8, pp. 1273-1282.

Chen, K. Y. (2016): Sliding mode minimum-energy control for a mechatronic motor-table system. *ASME Transactions on Mechatronics*, vol. 21, no. 3, pp. 1487-1495.

Chladny, R. R.; Koch, C. R. (2008): Flatness-based tracking of an electromechanical variable valve timing actuator with disturbance observer feedforward compensation. *IEEE Transactions on Control Systems Technology*, vol. 16, no. 4, pp. 652-663.

Dai, J.; Chang, S. (2014): Loss analysis of electromagnetic linear actuator. *International Journal of Applied Electromagnetics & Mechanics*, vol. 46, no. 3, pp. 471-482.

Elnagar, G.; Kazemi, M. A.; Razzaghi, M. (1995): The pseudospectral legendre method for discretizing optimal control problems. *IEEE Transactions on Automatic Control*, vol. 40, no. 10, pp. 1793-1796.

Fan, X. Y.; Liu, L.; Chang, S. Q.; Xu, J. T.; Dai, J. G. (2016): Electromagnetic valve train for gasoline engine exhaust system. *International Journal of Automotive Technology*, vol. 17, no. 3, pp. 361-367.

Fan, X.; Chang, S.; Liu, L.; Lu, J. (2016): Realization and optimization of high compression ratio engine with electromagnetic valve train. *Applied Thermal Engineering*, vol. 112, pp. 371-377.

Garg, D.; Patterson, M. A.; Hager, W. W.; Rao, A. V.; Benson, D. et al. (2017): An overview of three pseudospectral methods for the numerical solution of optimal control problems. *Advances in the Astronautical Sciences*, vol. 135, pp. 475.

Huang, M. S.; Hsu, Y. L.; Fung, R. F. (2012): Minimum-energy point-to-point trajectory planning for a motor-toggle servomechanism. *IEEE/ASME Transactions on Mechatronics*, vol. 17, no. 2, pp. 337-344.

Hey, J.; Teo, T. J.; Bui, V. P.; Yang, G.; Martinez-Botas, R. (2014): Electromagnetic actuator design analysis using a two-stage optimization method with coarse-fine model output space mapping. *IEEE Transactions on Industrial Electronics*, vol. 61, no. 10, pp. 5453-5464.

Kim, H.; Kim, B. K. (2014): Online minimum-energy trajectory planning and control on a straight-line path for three-wheeled omnidirectional mobile robots. *IEEE Transactions on Industrial Electronics*, vol. 61, no. 9, pp. 4771-4779.

Liu, L.; Chang, S. (2009): On feasibility of a moving coil electromagnetic valve actuator. *China Mechanical Engineering*, vol. 20, no. 19, pp. 2283-2287.

Liu, L. A. (2009): Analysis and design of a moving-coil electromagnetic valve actuator. *Automotive Engineering*, vol. 31, no. 8, pp. 733-736.

Liu, L.; Chang, S. (2011): Improvement of valve seating performance of engine's electromagnetic valvetrain. *Mechatronics*, vol. 21, no. 7, pp. 1234-1238.

Olyaie, M. S.; Razfar, M. R.; Wang, S.; Kansa, E. J. (2011): Topology optimization of a linear piezoelectric micromotor using the smoothed finite element method. *Computer Modeling in Engineering & Sciences*, vol. 82, no. 1, pp. 55-81.

Tan, C.; Li, B.; Ge, W.; Sun, B. (2018): Design and analysis of a bi-stable linear force actuator for directly-driven metering pump. *Smart Materials and Structures*, vol. 27, no. 10.

Wang, Y.; Ueda, K.; Bortoff, S. A. (2013): A hamiltonian approach to compute an energy efficient trajectory for a servomotor system. *Automatica*, vol. 49, no. 12, pp. 3550-3561.

Wang, Y.; Zhao, Y.; Bortoff, S. A.; Ueda, K. (2015): A real-time energy-optimal trajectory generation method for a servomotor system. *IEEE Transactions on Industrial Electronics*, vol. 62, no. 2, pp. 1175-1188.

Yang, Y. P.; Liu, J. J.; Ye, D. H.; Chen, Y. R.; Lu, P. H. (2013): Multiobjective optimal design and soft landing control of an electromagnetic valve actuator for a camless engine. *IEEE/ASME Transactions on Mechatronics*, vol. 18, no. 3, pp. 963-972.

Yang, S.; Cui, T.; Hao, X.; Yu, D. (2017): Trajectory optimization for a ramjet-powered vehicle in ascent phase via the gauss pseudospectral method. *Aerospace Science & Technology*, vol. 67, pp. 88-95.

Zhao, J. (2018): Distance control algorithm for automobile automatic obstacle avoidance and cruise system. *Computer Modeling in Engineering & Sciences*, vol. 116, no. 1, pp. 69-88.